Texture Representation Through Overlapped Multi-Oriented Tri-Scale Local Binary Pattern

FAWAD [1], (Student Member, IEEE), MUHAMMAD JAMIL KHAN[1], (Member, IEEE), MUHAMMAD ALI RIAZ[1], (Member, IEEE), HUMAYUN SHAHID[1], (Member, IEEE), MANSOOR SHAUKAT KHAN[2], YASAR AMIN [1], (Senior Member, IEEE), JONATHAN LOO [3], (Member, IEEE), AND HANNU TENHUNEN[4,5], (Member, IEEE)

[1]ACTSENA Research Group, Telecommunication Engineering Department, University of Engineering and Technology Taxila, Taxila 47050, Pakistan
[2]Mathematics Department, COMSATS University Islamabad, Islamabad 45550, Pakistan
[3]School of Computing and Engineering, University of West London, London W5 5RF, U.K.
[4]Department of Electronic Systems, Royal Institute of Technology (KTH), SE 16440 Stockholm, Sweden
[5]Department of Information Technology, TUCS, University of Turku, 20520 Turku, Finland

Corresponding author: Fawad (engr.fawad@students.uettaxila.edu.pk)

ABSTRACT This paper ideates a novel texture descriptor that retains its classification accuracy under varying conditions of image orientation, scale, and illumination. The proposed Overlapped Multi-oriented Tri-scale Local Binary Pattern (OMTLBP) texture descriptor also remains insensitive to additive white Gaussian noise. The wavelet decomposition stage of the OMTLBP provides robustness to photometric variations, while the two subsequent stages – overlapped multi-oriented fusion and multi-scale fusion – provide resilience against geometric transformations within an image. Isolated encoding of constituent pixels along each scale in the joint histogram enables the proposed descriptor to capture both micro and macro structures within the texture. Performance of the OMTLBP is evaluated by classifying a variety of textured images belonging to Outex, KTH-TIPS, Brodatz, CUReT, and UIUC datasets. The experimental results validate the superiority of the proposed method in terms of classification accuracy when compared with the state-of-the-art texture descriptors for noisy images.

INDEX TERMS Classification, geometric transformations, photometric variations, texture representation, wavelet decomposition.

I. INTRODUCTION

Human visual perception system banks heavily on structural components within an image for pattern classification and object recognition. Natural images, in general, consist of highly complected structures, modeling which remains a long-standing challenge. Accurate texture modeling and classification is crucial for a variety of modern-day applications, including medical imaging [1] and retrieval [2]. Agricultural produce such as herbs [3], fruits [4], leaves [5], rocks [6], mud [7], and wood [8], as well as industrial products including marble [9], and fabric [10] possess unique textural characteristics that provide basis for categorization into respective classes. Event detection [11], [12] biometric authentication [13], multimedia retrieval [14], landmark identification [15], and similar applications rely largely upon robust texture representation for attaining desirable system performance.

Textons are image micro-structures serving as building blocks that play a key role in the visual perception of texture by humans. The periodic repetition of textons with well-defined spacing and relative positioning imparts distinct textural characteristics to different regions within a digital image [16]. The aim is to identify statistical properties of the local image regions that, in turn, can be leveraged to evaluate differential maxima in the feature euclidean vector space. The robustness associated with texture classification process depends not only upon how accurately the image has been represented but also on the choice of underlying feature classifier and image similarity metric. Nearest Neighbor

Classifier (NNC) [17], Support Vector Machine (SVM) [18], and Nearest Subspace Classifier (NSC) [19] are widely used for feature classification. NSC is a definite improvement over NNC because the former does away with the problem of overfitting which the latter remains vulnerable to. Classifier regularization is achieved in NSC by taking into account the associated variance constraint parameter. Upon choosing a considerably low value of variance constraint, NSC effectively transforms into NNC in terms of classification performance. Owing to its advantages and superior performance, the proposed texture descriptor makes use of NSC for the purpose of feature classification [20].

An increasing number of present-day applications require attaining a higher texture classification accuracy. This, in turn, requires a stable and robust texture representation that is insensitive to geometric and photometric variations of the image. Traditionally, the said has been achieved by designing texture descriptors that are largely independent of changes taking place in the rotation, scale, and illumination. Such descriptors, however, struggle with attaining a high value of classification accuracy when the texture under investigation contains a large amount of noise.

This work ideates a new approach towards texture representation offering highly sought-after features including deterrence against additive white Gaussian noise, immunity against orientation changes, robustness to scale variation and insensitivity towards illumination changes. Deterrence against additive white Gaussian noise has been achieved by decomposing the input image into corresponding subbands using wavelet transform. Immunity against orientation changes is developed by including overlapped multi-oriented pixel fusion process. Robustness to scale variation is secured by incorporating multi-scale fusion in the descriptor. Insensitivity towards illumination is attained using normalization of relevant features.

The proposed descriptor holds immense appeal for deployment in various novel applications. For instance, autonomous person re-identification in distributed surveillance systems can potentially be improved using the proposed texture descriptor. By combating illumination changes and environmental noise, the descriptor is likely to enhance the classification accuracy in intelligent surveillance applications. Similarly, for emerging applications in aerial imaging, robustness offered by the proposed descriptor can potentially be leveraged for disaster evaluation and evacuee localization while maintaining reasonable classification accuracy.

The remaining discussion is organized as follows. Section II provides coverage of related work reported in the literature. Section III details the formulation of the proposed texture descriptor. In section IV, we describe the obtained results and their comparison with state-of-the-art texture models. The conclusion is drawn in section V of this paper.

II. RELATED WORK

In general, techniques developed for texture feature extraction can be broadly classified into two main categories [21]. The first category draws heavily from research in deep learning, where several models based upon Convolutional Neural Networks (CNNs) have been developed. Though such models allow for the extraction of texture features with relatively high accuracy, the massive amount of training data required makes the entire process both computationally expensive and time consuming. The second category relies upon hand-crafted techniques aimed at feature extraction, which largely remain independent of training data and function without much of a computational overhead [21]. In this category, extraction of discriminative features from the structural composition is crucial, and governs the degree of robustness offered by the resulting descriptor.

In hand-crafted feature extraction methods, several algorithms have been proposed during the last decade [22]. Among them, local binary pattern (LBP) [23] is the most widely used technique. LBP encodes the pixels of each segment by thresholding the same against intensity measure corresponding to the pixel in the center. LBP has captured the attention of researchers due to its computational efficiency, robustness to illumination as well as changes in orientation. However, LBP descriptor is sensitive to grayscale intensity inversion that might take place [24], [25]. Robustness to inverse gray-scale intensities is achieved in the complete local binary pattern (CLBP) [26] by incorporating magnitude and center components in the LBP description. CLBP still remains sensitive to illumination changes, necessitating the image be normalized as a pre-step in order to remove the effects of global intensity changes. Moreover, other variants of LBP such as dominant LBP (DLBP) [38], complete local binary count (CLBC) [52], complete dual-cross pattern (CDCP) [47], local directional ZigZag pattern (LDZP) [48], and local morphological pattern (LMP) [56] have also been developed for various applications. These methods, however, are sensitive to noise in the texture, and the feature values of such descriptors vary in a non-uniform manner in response to changes in scale. The DLBP offers better accuracy by utilizing only the most frequently occurring binary pattern of LBP. On the downside, the descriptor neglects discriminant macro-structures present in the texture. It is worth noting that both CDCP and LDZP can only extract the isotropic microstructures, which cannot represent the textual characteristics effectively. Median robust extended local binary pattern (MRELBP) has been developed [29] to capture the micro- and macro-structures of the image. Though this approach offers lowered computational complexity and feature dimensionality, it still requires non-local median pixel sampling. Complete joint-scale local binary pattern (CJLBP) [27] is developed to include neighbors at multiple scales around the center pixel in CLBP. The CJLBP consider multiples scale of the texture, which improves the classification accuracy for scale variations in the input image at the cost of computational complexity.

Noise, which affects the micro-geometric structures, can also degrade the classification accuracy. Hence, noise tolerant texture representation has sparked interest in the research

community. Local ternary pattern (LTP) [40] is developed for noisy texture representation. The feature vector associated with LTP is not vulnerable to gray-scale inversion. At the same time, LTP functions by decomposing a texture locally into positive and negative binary patterns. This constituent step has been criticized as an inefficient approach towards texture decomposition [41]. A peculiar diamond sampling structure-based local adaptive binary pattern (DLABP) is presented in [30]. This method has obtained efficiency and simplicity in noisy texture representation by introducing diamond-shaped sampling, adaptive quantization, and gray level averaging across a radial direction. The method performs well for noisy texture of the Outex database. However its performance degrades when test on several other texture databases.

Noise resistant local binary pattern (NRLBP) [50] can perform texture classification in the presence of noise with high accuracy. However, the noise tolerance capability of NRLBP remains unsatisfactory in many applications [29]. In addition, the memory requirements of NRLBP increases exponentially with the number of sample points [51]. In [28], binary rotation invariant and noise tolerant (BRINT) descriptor has been developed which, as the name suggests, combats changes in rotation as well as noise within the texture. Speaking of limitations, BRINT undergoes a rapid increase in feature dimensionality due to its multi-scale approach and is also sensitive to illumination-related changes.

Varma and Zisserman Maximum Response (VZ-MR8), [42], and Varma and Zisserman Patch (VZ-Patch) [43] describe both micro- and macro-textures by employing dense response of multiple spatial filters. VZ-MR8 and VZ-Patch descriptors provide poor results in comparison to LMP with high computational complexity. LBPV [37] utilizes local contrast information to describe the texture in the input image. Moreover, it also includes global rotation-invariant texture matching to improve the classification accuracy. The main drawback is high dimensionality associated with the resulting feature vector.

This work presents a novel texture descriptor, offering highly-desirable features of insensitivity to variation in the factors enlisted below, even in the presence of additive white Gaussian noise:

- Illumination
- Scale
- Orientation

The underlying algorithmic details for the proposed texture descriptor are presented section-wise.

III. PROPOSED TEXTURE DESCRIPTOR

The focus of the proposed approach is to formulate a texture descriptor robust to variation in illumination, scale, and rotation. CJLBP is taken as a starting point, wherein multi-scale fusion is performed to create a combined 3×3 patch of the pixels. The above is carried out by applying an averaging operation around all defined radii corresponding to a segment. Sign and magnitude components are calculated by subjecting the multi-scale fused patch to the local difference sign magnitude transform (LDSMT). The operators CJLBP_S, CJLBP_M, and CJLBP_C representing the histogram of the center, magnitude and sign components of the image, are computed. Thereafter, the operators are combined in different ways to create multiple variants of the parent technique. CJLBP_MC is the result of combining CJLBP_M and CJLBP_C. Likewise, CJLBP_S_MC, CJLBP_SM, and CJLBP_SMC have been demonstrated to yield good classification accuracy [27].

The proposed framework is divided into three stages. The first stage of the proposed method provides deterrence against additive white Gaussian noise, and immunity against the orientation changes. The second stage makes the descriptor robust to scale variations. The third stage normalizes the extracted features along each radius. In the third stage, the descriptor becomes insensitive to illumination changes. The detail description of each stage is available in the following subsections.

A. STAGE 1

In the proposed technique, the image under investigation is first decomposed into its sub-bands using two-dimensional discrete wavelet transform (2D-DWT). The approximation coefficients are obtained through dmey (Discrete approximation of Meyer) waveform of the wavelet at single level decomposition. Values of the feature vector are extracted from the approximated version of an image. An individualized segment of the low frequency sub-band (LL) is calculated using Eq. (1) given as:

$$Y_{r,c} = LL(r + u, c + v) \tag{1}$$

where $Y_{r,c}$ shown in Fig. 1 (a) represents the segment of the approximated image corresponding to center pixel. The row (r) and column (c) define the location of the segment in the approximated image. The pixels of the segment $Y_{r,c}$ are shown with the help of symbol J_{θ}^{s}. The subscript θ is the orientation angle, while the superscript s represents the radius. Since it is not possible to extract a segment $Y_{r,c}$ near the periphery of the image, r and c are therefore constrained to vary over a certain range defined by the interval $[1 + R_{max}$ x_n-$R_{max}]$ and $[1+R_{max}$ y_n-$R_{max}]$, respectively. x_n, y_n represent the last row and column position of the approximated image, while R_{max} is the maximum radius of the segment $Y_{r,c}$. Variables u and v in Eq. (1) define the coordinates of the segment in the approximated image. Note that both u and v span over a range of $[-R_{max} + R_{max}]$. Dimensions of $Y_{r,c}$ in pixels equal $(2R_{max} + 1) \times (2R_{max} + 1)$ segment of the approximation.

The overlapped multi-oriented pixel fusion process, shown in Fig. 1 (b), creates a topological structure of 8 samples for all 3 scales shown in Fig. 1 (c). Overlapped multi-oriented pixel fusion process is performed over the pixels laying at radius 2 and 3 are shown in Eq. (2) and (3). Sample points P_k^3, P_k^2, and P_k^1 in Eq. (2), (3), and (4) represent the topological

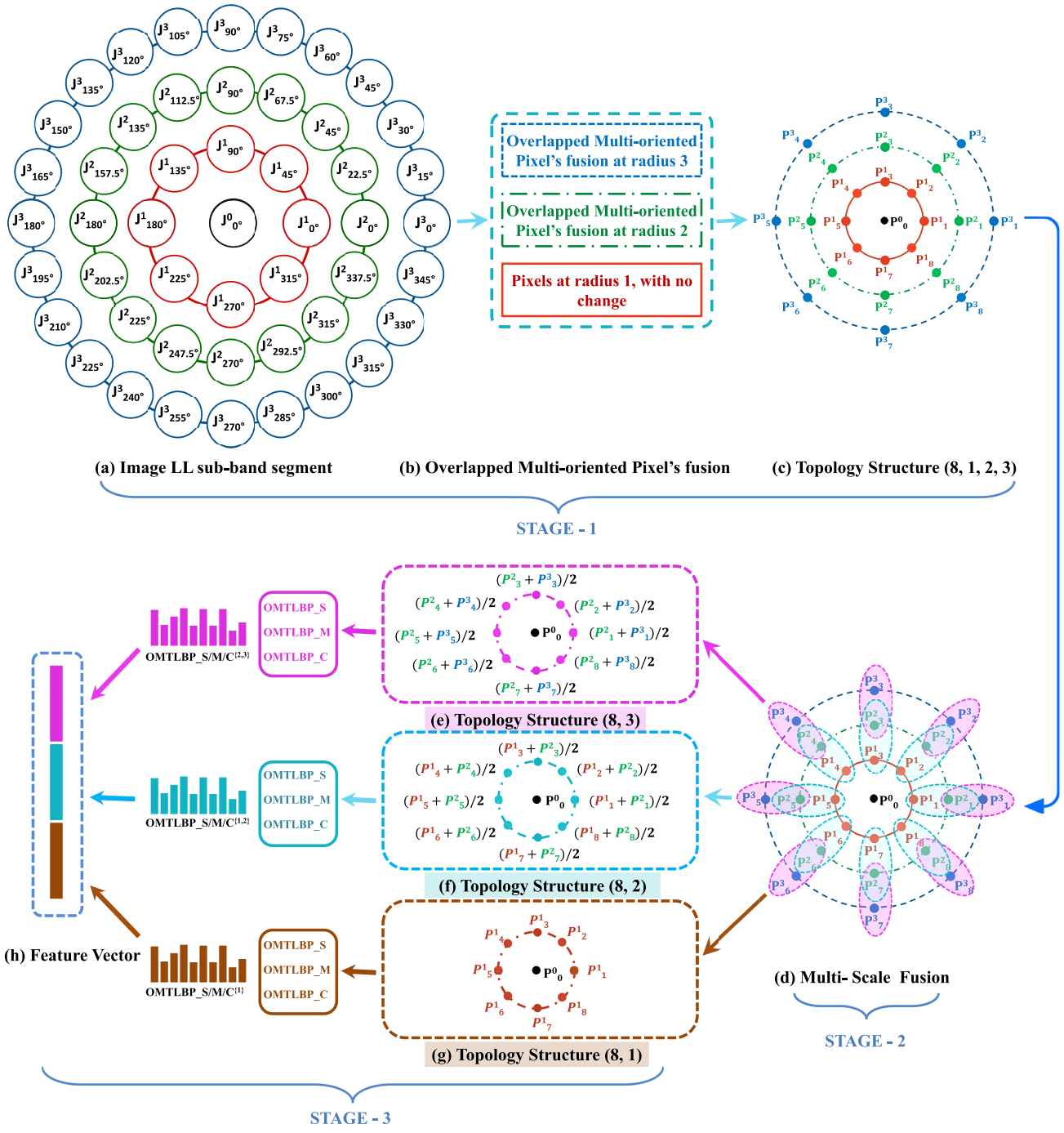

FIGURE 1. Framework of our proposed texture representation approach.

structure of 8 samples with radius 3, 2, and 1 respectively.

$$P_k^3 = \left\{ \frac{\left(\sum_{i=0}^{6} (J^3_{0°+15°(i)+45°(k-2)}) \right)}{7} \right\}_{k=1}^{8} \tag{2}$$

$$P_k^2 = \left\{ \frac{\left(\sum_{i=0}^{4} (J^2_{0°+22.5°(i)+45°(k-2)}) \right)}{5} \right\}_{k=1}^{8} \tag{3}$$

$$P_k^1 = \left\{ J^1_{0°+45°(k-1)} \right\}_{k=1}^{8} \tag{4}$$

B. STAGE 2

In order to make the descriptor robust to scale variations, a multi-scale fusion operation is performed in two steps which are shown in Fig. 1 (d) and summarized in algorithm 1. In the first step, samples at radii 1 and 2 are fused through mean operation, while in the second step samples belonging to radii 2 and 3 are combined together. For each segment $Y_{r,c}$ the multi-scale fusion depends on the set of radius R and sample point k. The multi-scale fusion is represented

using Eq. (5).

$$\widetilde{y}_{r,c} = \left\{ \frac{\sum_{i=(n-1)}^{n} \left(P_k^i\right)}{2} \right\}_{k=1}^{8} \tag{5}$$

where P_k^i represents the k^{th} pixel intensity at radius R_i of the topological structure in Fig. 1 (c). $\widetilde{y}_{r,c}$ denotes the multi-scale fused patch with topological structure (8, 3), (8, 2) and (8, 1) of the Fig. 1 (e), (f), and (g) respectively.

C. STAGE 3

In the third stage feature vectors are extracted from each topological structure shown in Fig. 1 (e), (f), and (g). The local difference sign-magnitude transform (LDSMT) is used to calculate the sign and magnitude component from the $\widetilde{y}_{r,c}$.

$$d_{r,c} = \left\{ \widetilde{y}_{r,c}^k - C_{r,c} \right\}_{k=1}^{P} \tag{6}$$

$$d_{r,c} = \left\{ s_{r,c}^k \times m_{r,c}^k \right\}_{k=1}^{P} \quad \text{and} \quad \begin{cases} s_{r,c}^k = sign(d_{r,c}^k) \\ m_{r,c}^k = |d_{r,c}^k| \end{cases} \tag{7}$$

where $d_{r,c}$ denotes the set of local difference, $\widetilde{y}_{r,c}^k$ represents the k^{th} sample point of the multi-scale fused patch, and $C_{r,c}$ represents the intensity value of the center pixel corresponding to segment $Y_{r,c}$. $s_{r,c}^k$ represents the k^{th} sign component having a value equal to 1 when $d_{r,c}^k$ is greater than or equal to 0, and -1 when $d_{r,c}^k$ is less than 0. The magnitude component $m_{r,c}$ stores the absolute values of the local difference $d_{r,c}$ The rotation invariant operator OMTLBP_S$_{P,R}^{riu2}$ is obtained using the sign component $s_{r,c}$ of the local difference $d_{r,c}$. Its encoding is formulated as LBP$_{P,R}^{riu2}$ [23]. The rotation invariant operator OMTLBP_M$_{P,R}^{riu2}$ shown in Eq. (8) is obtained using the magnitude component of the local difference $d_{r,c}$.

$$OMTLBP\_M_{P,R}^{riu2} = \begin{cases} \psi(m_{r,c}^k, \mu_m), & \text{if } U\_M_{P,R} \leq 2 \\ P+1, & \text{otherwise} \end{cases} \tag{8}$$

$$\begin{aligned} U\_M_{P,R} = {} & |\psi(m_{r,c}^{P-1}, \mu_m) - \psi(m_{r,c}^0, \mu_m)| \\ & + \sum_{k=1}^{P-1} |\psi(m_{r,c}^k, \mu_m) - \psi(m_{r,c}^{k-1}, \mu_m)| \end{aligned} \tag{9}$$

where $\psi(x, y)$ is 1 for x greater than or equal to y and $\psi(x) = 0$ for $x < y$. The $m_{r,c}^k$ is the k^{th} magnitude component and μ_m is the mean value of the magnitude component of the segment at location (r,c) of the input image. In addition to the sign and magnitude pattern, the center pixel's grey level OMTLBP_C is also considered. This is formulated as

$$OMTLBP\_C_{P,R} = \psi(C_{r,c}, \mu_I) \tag{10}$$

where μ_I represents the mean value of the whole input image. The joint combination of operators OMTLBP_S$_{P,R}^{riu2}$, OMTLBP_M$_{P,R}^{riu2}$, and OMTLBP_C$_{P,R}$ is represented by OMTLBP_SMC$_{P,R}^{riu2}$.

The train and test feature vectors are obtained using the operator OMTLBP_SMC$_{P,R}^{riu2}$. Chi-square distance is used as a dissimilarity measure, and the classification accuracy is obtained using Eq. (11).

$$Accuracy = \frac{TP + TN}{TP + FP + TN + FN} \tag{11}$$

where TP stands for true positive, TN signifies true negative, FN corresponds to false negative, and FP denotes false positive samples of the test dataset. It is worth-noting that the classification accuracy of a descriptor reflects its ability to categorize textured images into respective classes, and is a key metric to evaluate the performance.

Algorithm 1 Extract OMTLBP_SMC Feature Vector

Input : Input image I of size M × N
Output : Feature Vector: OMTLBP_SMC
Initialization: The parameters as $R_{max} = 3$, $r = R_{max} + 1$, and $c = R_{max} + 1$

```
Apply 2D-DWT on I ;
Extract the Approximation (LL);
for r ≤ (M − R_max) do
    for c ≤ (N − R_max) do
        Extract the segment Y_{r,c} using Eq. (1);
        Compute P_k^3, P_k^2, and P_k^1 described through
        Eq. (2), (3), and (4);
        Compute ỹ_{r,c} through Eq. (5) for the set of {1,
        2} and {2, 3};
        for each topological structure do
            Compute LDSMT by Eq. (6) and (7) ;
            Compute sign S, magnitude M, and center C
            component;
        end
        increment c;
    end
    increment r;
end
Compute OMTLBP_S, OMTLBP_M, and OMTLBP_C
from the component S,M, and C;
Concatenate all operators to get OMTLBP_SMC;
```

IV. EXPERIMENTAL RESULTS AND ANALYSIS

The experimental validation of the proposed technique is carried out on multiple texture datasets including Outex [31], Brodatz Album [32], CUReT [33], and KTH-TIPS [35]. The accuracy of OMTLBP descriptor is validated by employing the k-fold cross-validation procedure. Nearest subspace classifier (NSC), with Chi-Square (χ^2) distance, is employed for test feature classification. The k-fold cross-validation scheme requires a set of train and test features. In the proposed novel approach, the feature set of each class is re-arranged randomly before splitting the same into train and test set. In k-folds with k = 10, the k−1 folds train data, while the remaining features are used as test data for classification. The final cross-validation accuracy is the mean of all classification accuracies obtained in k number of rounds.

TABLE 1. Texture databases overall summary.

Parameters	TC10 (Outex) [31]	TC12 (Outex) [31]	KTH-TIPS [35]	Brodatz [32]	CUReT [33]	UIUC [34]
Rotation	✓	✓	✓	✓	✓	✓
Illumination changes		✓	✓		✓	
Scale changes			✓	✓		✓
Classes	24	24	10	32	61	25
Size in Pixels	128×128	128×128	200×200	64×64	200×200	640×480
Samples per Class	180	200	81	64	92	40
AWGN included with SNR (dB)	40 - 5	40 - 5	40 - 5	40 - 5	40 - 5	40 - 5
Total Samples	4320	4800	810	2048	5612	1000

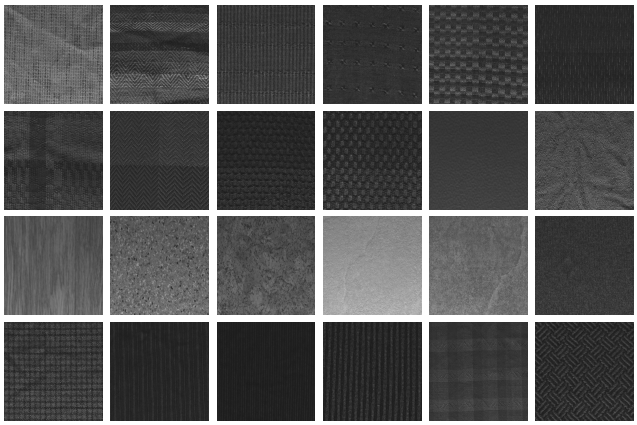

FIGURE 2. Texture samples from outex database [31].

A. OUTEX

Outex database consists of 24 different homogeneous texture classes depicted in Fig. 2. The illumination and rotation invariance of OMTLBP is examined by employing three test suites, TC10, TC12 000, and TC12 001 from the Outex database. For all test suites, the classifier is trained using 20 reference images with an orientation angle of 0° and illumination condition 'inca', which makes a total of 480 samples. The difference between these three test suites is in their test data. In Outex TC10, 3840 samples with rotation angles 5°, 10°, 15°, 30°, 45°, 60°, 75°, and 90° with illumination condition 'inca', are used for testing the classifier. In Outex TC12 000 and Outex TC12 001, the classifier is tested with all 4320 images from fluorescent and sunlight lighting, respectively. The dataset has been summarized in Table 1.

Extensive experimentation has been carried out on the previously mentioned test suites of the Outex database. The results of the proposed OMTLBP is compared with a number of recently-reported descriptors. The proposed texture descriptor has attained the highest classification accuracy when tested on all test suits in the Outex database. The average classification accuracy of the proposed descriptor remains 0.02%, 0.2%, 0.91%, and 1.39% higher than LDZP, CDCP, CJLBP_SMC, BRINT_CS_CM respectively. Inclusion of noise affects the micro-structures, leading to reduced inter class variations in the texture. The proposed texture descriptor is also evaluated on noisy textured images. Table 2 describes the comparative results in term of classification accuracy (%). The table shows that the proposed descriptor with NSC classifier outperforms the other techniques. Upon addition of Gaussian noise (AWGN) with signal-to-noise ratio (SNR) 100 dB, 30 dB, 15 dB, and 5 dB, classification accuracy of 99.96%, 99.84%, 99.80%, and 99.75% has been demonstrated using the proposed method. The initial wavelet decomposition stage renders the proposed OMTLBP descriptor robust against noise. Wavelet decomposition of the input image via demy waveform breaks the image into approximation and detail coefficients. The coefficients of the approximation provide distinctive features, which maximize the inter-class variation of the feature set.

B. BRODATZ

Brodatz dataset [32] consists of total 2048 sample images of 32 homogeneous texture classes. The dataset samples have variations in their scale and orientation. Each sample of the dataset is divided into 25 non-overlapping segments of size 128 × 128 pixels. The patches are further down-sampled into 64×64 pixels. Each texture class contains a total of 64 sample images. The dataset image of each class is labeled with four different properties namely, that are normal, rotated, scaled, and scaled with rotation. The dataset is summarized in Table 1. Few randomly selected color samples of the database have been presented in Fig. 3. The difference in scale and orientation may create variations in the micro-texture of the image. The images of the dataset consist of grass, wood, water, gain, bricks, sand, and many other naturally-occurring texture-rich objects.

The classification presented in Table 3 depicts that the proposed OMTLBP descriptor, when applied to images in the Brodatz database outperforms most of the other techniques. The proposed descriptor with classification accuracy 99.17% results in a percentage improvement of 0.01%, 4.37%, 4.55%, and 4.57% when compared with DLBP, CLBP_SMC,

TABLE 2. Performance analysis (%) on TC10 (Outex) and TC12 (Outex) [31].

Technique	Classifier	TC10 (Outex)	TC12h (Outex)	TC12t (Outex)	Average
$LBP^{NT}_{R,N}$ [36]	NNC	99.24	96.18	94.28	96.56
MRELBP [29]	NNC	91.17	84.95	87.01	87.71
DLABP [30]	NNC	99.04	95.35	94.93	96.44
PTP [44]	NNC	99.56	98.08	97.94	98.52
LDDP [45]	NNC	97.89	93.40	95.30	95.53
DRLBP [46]	NNC	99.19	95.80	96.72	97.23
CDCP [47]	NNC	99.76	99.82	99.62	99.72
LDZP [48]	NNC	99.95	99.93	99.82	99.90
NRLBP [50]	NNC	93.44	86.13	87.38	88.98
CLBC CSM [52]	NNC	98.96	95.37	94.72	96.35
DLBP+NGF [38]	SVM	99.1	93.2	90.4	94.23
CLBP_S/M/C [26]	NNC	98.93	92.29	90.30	93.84
$CJLBP\_SMC^{riu2}$ [27]	NNC	99.77	98.59	98.68	99.01
$LBPV^{riu2}_{R,N}$ [37]	NNC	91.56	77.01	76.62	81.73
$DLBP_{R=3,N=24}$ [38]	SVM	98.10	87.40	91.60	92.36
BRINT_CS_CM [28]	NNC	99.35	97.69	98.56	98.53
VAR [39]	NNC	90.00	64.35	62.93	72.42
LBP [23]	SVM	97.60	85.30	91.30	91.40
LTP [40]	NNC	76.06	63.42	62.56	67.34
VZ-MR8 [42]	NSC	93.59	92.82	92.55	92.99
VZ-Patch [43]	NSC	92.00	92.06	91.41	91.82
Proposed OMTLBP	**NSC**	**99.96**	**99.98**	**99.82**	**99.92**

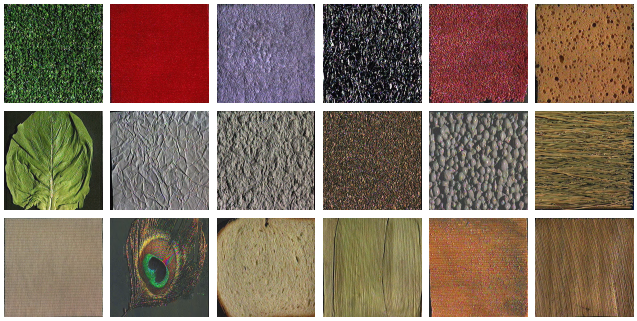

FIGURE 3. Texture samples from Brodatz album [32].

VZ-MR8, and LBPHF_S, respectively. The classification accuracy of the proposed descriptor stands at 99.17%, which is slightly lower than BRINT_CS_CM. On the other hand, BRINT_CS_CM comprehensively falls short when applied on a number of significant databases when compared with the proposed texture descriptor. This wider adaptability of the proposed texture descriptor validates its efficacy as a leading choice in the new-age of texture classification applications.

C. CUReT

The CUReT database [33] has a total of 61 texture classes. Each class contains 92 sample images. The database is designed by including a large intra-class variation in the samples, making it the main reason why this particular dataset is heavily used for texture descriptor validation purpose [49]. The images of the database have a difference in illumination. The scale of the images in each class is kept constant. All 92 samples from 61 texture classes are densely divided

TABLE 3. Comparison of classification accuracy (%) on KTH-TIPS [35], Brodatz [32], CUReT [33] and UIUC [34].

Technique	Classifier	KTH-TIPS [35]	Brodatz [32]	CUReT [33]	UIUC [34]
LBPV [37]	NNC	95.50	93.80	94.00	-
CLBP_SMC [26]	NNC	97.19	94.80	97.40	93.26
$CJLBP\_SMC^{riu2}$ [27]	NNC	-	-	97.51	95.13
$DLBP_{R=3,N=24}$ [38]	SVM	86.99	99.16	84.93	60.73
$LBP^{riu2}_{1,8}$ [36]	NNC	95.17	91.60	95.84	76.88
MRELBP [29]	NNC	-	-	94.11	86.79
DLABP [30]	NNC	-	-	96.75	92.36
BRINT_CS_CM [28]	NNC	97.75	99.22	97.06	93.26
LBP [36]	SVM	82.67	82.16	80.63	55.26
SSLBP [53]	NNC	97.80	-	98.55	97.02
VZ-MR8 [42]	NSC	94.50	94.62	97.43	93.59
LBPHF_S [54]	NNC	97.00	94.60	95.90	-
COALBP [55]	NNC	97.00	94.20	98.00	-
LMP [56]	NNC	98.37	-	98.11	-
VZ-Patch [43]	NSC	92.40	87.10	98.03	97.83
Proposed OMTLBP	**NSC**	**98.58**	**99.17**	**98.58**	**97.86**

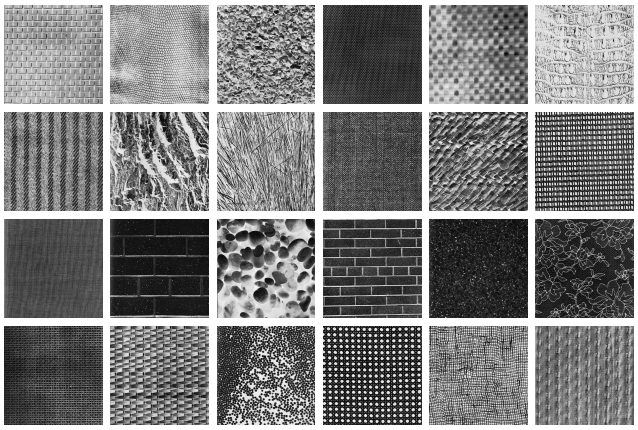

FIGURE 4. Texture samples from CUReT [33].

into 200 × 200 local regions, and each segment is converted into grayscale. The dataset is summarized in Table 1. Few randomly selected samples of the dataset have been presented in Fig. 4.

The classification accuracy of the proposed descriptor on CUReT dataset is 98.58%, which is 0.03%, 0.47%, 0.55%, and 0.58% higher than SSLBP, LMP, VZ-Patch, and COALBP descriptor respectively. The classification accuracy presented in Table 3 highlights the superiority of the proposed texture descriptor over recently reported techniques.

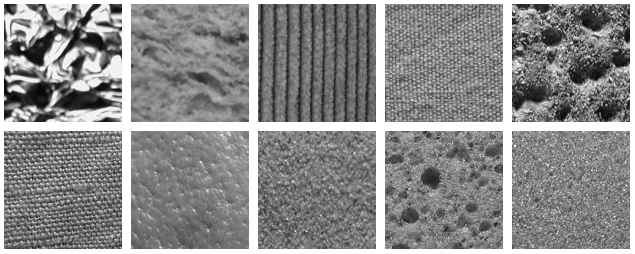

FIGURE 5. Random samples from KTH-TIPS [35] database.

D. KTH-TIPS

Ten texture classes of the CUReT database [33] have been extended to create KTH-TIPS dataset [35] as shown in Fig. 5. The database has a total of 810 texture images categorized in ten different classes. Each class contains a total of 81 samples images. The total size of each sample is 200 × 200. All images are in grayscale. The texture samples of each class have three different poses, four illumination types, and nine scales. The dataset is summarized in Table 1. The classification accuracy in Table 3 shows that the OMTLBP outperforms all other approaches mentioned in the table in terms of classification accuracy. The proposed approach exhibits 98.58% accuracy which is 0.21%, 0.78%, 0.83%, 1.39%, 1.58%, and 1.58% higher than LMP, SSLBP, BRINT_CS_CM, CLBP_SMC, LBPHF, and COALBP respectively.

E. UIUC DATABASE

The UIUC database [34] consists of 25 different texture classes collected from various materials. Each class of the dataset includes 40 images with resolution 640 × 480. A few random samples from the dataset are in Fig. 6. The images of each class have variations in scale and viewpoint. Moreover, the images have non-rigid deformation and illumination changes. Half of the random samples from each class is selected for training, while the remaining half images are used as test data.

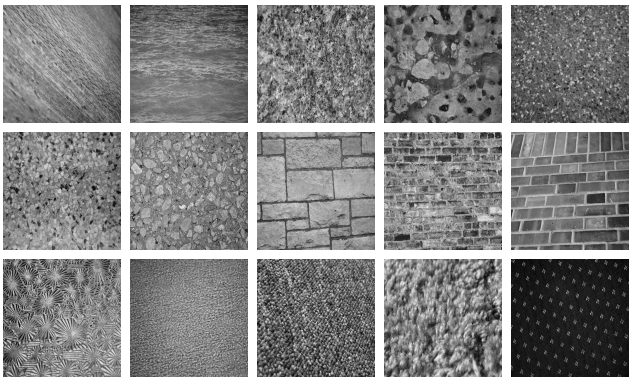

FIGURE 6. Random samples from UIUC [35] database.

The results presented in Table 3 proposed OMTLBP_SMC provides 0.03%, 0.84%, 2.73%, and 4.27% higher classification accuracy for VZ-Patch, SSLBP, CJLBP_SMC, and VZ-MR8 respectively.

The results achieved from the experimental setup reveal that the classification accuracy of the operator OMTLBP_SMC$^{riu2}_{P,R}$ is high for the set of radius R = 1, 2, and 3 with the sampling point value of 8. The comparison of classification accuracy obtained with various combinations of radius and sample points using the same databases is shown in Table 2 and 3. The results reported in Fig. 7 (a)-(d), show the proposed descriptor is much better than recently reported descriptors applied on the Outex, Brodatz, CUReT, and UIUC dataset in the presence of additive Gaussian noise. The noise with zero mean and standard derivation σ = (40, 30, 15, 5) dB is included in the texture before the validation process of Fig. 7. The dimension of the proposed descriptor in comparison to the recently reported approaches is presented in Fig. 8. The dimensionality of the proposed descriptor stands at 600 variables, which is lower than that offered by most recently developed descriptors.

Table 2 and 3 show the classification performance of different texture techniques with various scales R and sampling points P. The proposed OMTLBP_SMC$^{riu2}_{P,R}$ with wavelet type 'dmey' provides more robustness to additive white Gaussian noise as compared to other recently developed approaches. OMTLBP_SMC$^{riu2}_{P,R}$ with sample point 8 and radius set 1, 2, and 3, provides the average classification accuracy of 99.92%, 98.58%, 99.17%, 98.58%, and 97.86% with Outex [31], KTH-TIPS [35], Brodatz [32], CUReT [33],

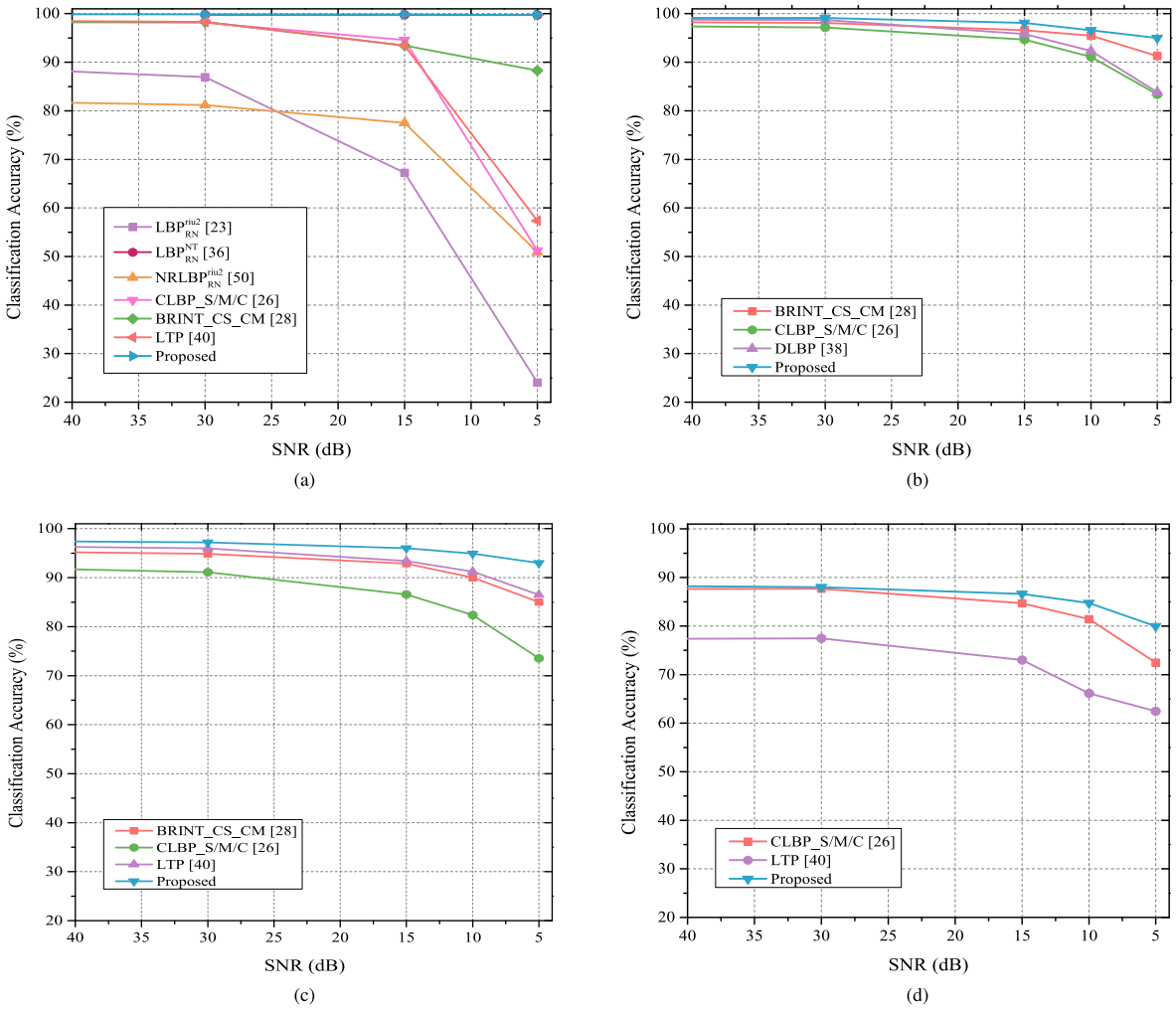

FIGURE 7. **Noisy texture classification on various publicly available databases. (a) Outex dataset [31]. (b) Brodatz dataset [32]. (c) CUReT dataset [33]. (d) UIUC database [34].**

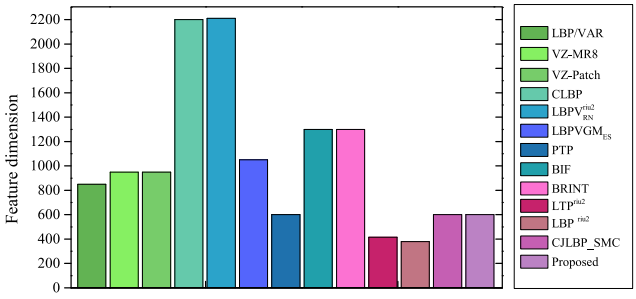

FIGURE 8. **Comparison of various texture descriptor's dimensionality.**

and UIUC [34] respectively that is better than all other combinations of radius for the same descriptor.

V. CONCLUSION

A novel texture descriptor, Overlapped Multi-oriented Triscale Local Binary Pattern (OMTLBP), is proposed in this work. The proposed descriptor is insensitive to a wide range of variations in image scale, illumination, and orientation. OMTLBP descriptor is also resilient to additive white Gaussian noise with SNR of up to 5 dB. This has been attained by decomposing the texture under investigation into its corresponding sub-bands. The OMTLBP contains the Overlapped Multi-oriented fusion that transforms each input segment of the image into eight sample points. The process imparts rotation invariant features to the proposed descriptor. Multi-scale fusion is also performed to merge the pixels along the radius in three different combinations. Doing so secures the sought-after property of scale invariance for the formulated descriptor. Moreover, the process of feature normalization has also been applied to achieve illumination invariance while designing the proposed texture descriptor.

When evaluated on publicly available texture databases, the proposed texture descriptor offers improved classification accuracy under conditions of geometric and photometric variations. In particular, comparison with four leading texture descriptors is performed for the case of Outex dataset where the average classification accuracy has been improved by 0.02% when compared with LDZP. Similarly, upon considering Brodatz dataset, an increase in average classification

accuracy is reported by 0.01% when compared with DLBP. On taking the CURET dataset into account, an improvement in classification accuracy has been reported by 0.03% in comparison with SSLBP. Upon analyzing texture images from KTH-TIPS, increase in average classification accuracy of 0.1% to that of LMP has been demonstrated. Finally, texture images from UIUC database have also been scrutinized wherein a performance improvement in terms of average classification accuracy is increased by 0.03% of VZ-Patch descriptor.

The descriptor holds potential for deployment across a broad array of applications related to texture classification including personnel re-identification in distributed video surveillance systems, search and localization tasks in aerial surveillance, and so on.

REFERENCES

[1] P. M. Pradhan, C. H. Cheng, and J. R. Mitchell, "A region of interest based approach for texture analysis of medical images in space–frequency domain," *Biomed. Signal Process. Control*, vol. 51, pp. 222–234, May 2019.

[2] F. Alaei, A. Alaei, U. Pal, and M. Blumenstein, "A comparative study of different texture features for document image retrieval," *Expert Syst. Appl.*, vol. 121, pp. 97–114, May 2019.

[3] R. Branca, S. Triantaphillidou, and P. Burns, "Texture MTF from images of natural scenes," *Electron. Imag.*, vol. 2017, no. 12, pp. 113–120, 2017.

[4] A. Bonneau *et al.*, "Impact of fruit texture on the release and perception of aroma compounds during *in vivo* consumption using fresh and processed mango fruits," *Food Chem.*, vol. 239, pp. 806–815, Jan. 2018.

[5] A. Riaz, S. Farhan, M. A. Fahiem, and H. Tauseef, "An ensemble classifier based leaf recognition approach for plant species classification using leaf texture, morphology and shape," *Nucleus*, vol. 55, no. 1, pp. 1–7, 2018.

[6] D. A. Jerram, K. J. Dobson, D. J. Morgan, and M. J. Pankhurst, "The petrogenesis of magmatic systems: Using igneous textures to understand magmatic processes," in *Volcanic and Igneous Plumbing Systems*. Elsevier, 2018, ch. 8, pp. 191–229. doi: 10.1016/B978-0-12-809749-6.00008-X.

[7] W. Wu, Q. Yang, J. Lv, A. Li, and H. Liu, "Investigation of remote sensing imageries for identifying soil texture classes using classification methods," *IEEE Trans. Geosci. Remote Sens.*, vol. 57, no. 3, pp. 1653–1663, Mar. 2018.

[8] R. Ren, T. Hung, and K. C. Tan, "A generic deep-learning-based approach for automated surface inspection," *IEEE Trans. Cybern.*, vol. 48, no. 3, pp. 929–940, Mar. 2018.

[9] A. Seul and K. Okarma, "Classification of textures for autonomous cleaning robots based on the GLCM and statistical local texture features," in *Proc. Comput. Sci. On-Line Conf.* Cham, Switzerland: Springer, 2018, pp. 405–414.

[10] Q. Huangpeng, H. Zhang, X. Zeng, and W. Huang, "Automatic visual defect detection using texture prior and low-rank representation," *IEEE Access*, vol. 6, pp. 37965–37976, 2018.

[11] X. Chang, Z. Ma, Y. Yang, Z. Zeng, and A. G. Hauptmann, "Bi-level semantic representation analysis for multimedia event detection," *IEEE Trans. Cybern.*, vol. 47, no. 5, pp. 1180–1197, May 2017.

[12] X. Chang, Y.-L. Yu, Y. Yang, and E. P. Xing, "Semantic pooling for complex event analysis in untrimmed videos," *IEEE Trans. Pattern Anal. Mach. Intell.*, vol. 39, no. 8, pp. 1617–1632, Aug. 2017.

[13] Z. Li, F. Nie, X. Chang, and Y. Yang, "Beyond trace ratio: Weighted harmonic mean of trace ratios for multiclass discriminant analysis," *IEEE Trans. Knowl. Data Eng.*, vol. 29, no. 10, pp. 2100–2110, Oct. 2017.

[14] L. Xie, L. Zhu, and G. Chen, "Unsupervised multi-graph cross-modal hashing for large-scale multimedia retrieval," *Multimedia Tools Appl.*, vol. 75, no. 15, pp. 9185–9204, 2016.

[15] L. Zhu, J. Shen, X. Liu, L. Xie, and L. Nie, "Learning compact visual representation with canonical views for robust mobile landmark search," in *Proc. Int. Joint Conf. Artif. Intell.*, 2016, pp. 3959–3965.

[16] U. R. Acharya *et al.*, "A novel algorithm for breast lesion detection using textons and local configuration pattern features with ultrasound imagery," *IEEE Access*, vol. 7, pp. 22829–22842, 2019.

[17] B. Caputo, E. Hayman, M. Fritz, and J.-O. Eklundh, "Classifying materials in the real world," *Image Vis. Comput.*, vol. 28, no. 1, pp. 150–163, 2010.

[18] J. Xu, C. Xu, B. Zou, Y. Y. Tang, J. Peng, and X. You, "New incremental learning algorithm with support vector machines," *IEEE Trans. Syst., Man, Cybern. Syst.*, to be published.

[19] J. Wright, A. Y. Yang, A. Ganesh, S. S. Sastry, and Y. Ma, "Robust face recognition via sparse representation," *IEEE Trans. Pattern Anal. Mach. Intell.*, vol. 31, no. 2, pp. 210–227, Feb. 2009.

[20] C. J. Veenman and M. J. T. Reinders, "The nearest subclass classifier: A compromise between the nearest mean and nearest neighbor classifier," *IEEE Trans. Pattern Anal. Mach. Intell.*, vol. 27, no. 9, pp. 1417–1429, Sep. 2005.

[21] P. Simon and V. Uma, "Review of texture descriptors for texture classification," in *Data Engineering and Intelligent Computing*. Singapore: Springer, 2018, pp. 159–176.

[22] A. Humeau-Heurtier, "Texture feature extraction methods: A survey," *IEEE Access*, vol. 7, pp. 8975–9000, 2019.

[23] T. Ojala, M. Pietikäinen, and T. Mäenpää, "Multiresolution gray-scale and rotation invariant texture classification with local binary patterns," *IEEE Trans. Pattern Anal. Mach. Intell.*, vol. 7, pp. 971–987, Jul. 2002.

[24] T. Song, L. Xin, C. Gao, G. Zhang, and T. Zhang, "Grayscale-inversion and rotation invariant texture description using sorted local gradient pattern," *IEEE Signal Process. Lett.*, vol. 25, no. 5, pp. 625–629, May 2018.

[25] M. Hu, Y. Zheng, C. Yang, X. Wang, L. He, and F. Ren, "Facial expression recognition using fusion features based on center-symmetric local octonary pattern," *IEEE Access*, vol. 7, pp. 29882–29890, 2019.

[26] Z. Guo and D. Zhang, "A completed modeling of local binary pattern operator for texture classification," *IEEE Trans. Image Process.*, vol. 19, no. 6, pp. 1657–1663, Jan. 2010.

[27] X. Wu and J. Sun, "Joint-scale LBP: A new feature descriptor for texture classification," *Vis. Comput.*, vol. 33, no. 3, pp. 317–329, 2017.

[28] L. Liu, Y. Long, P. W. Fieguth, S. Lao, and G. Zhao, "BRINT: Binary rotation invariant and noise tolerant texture classification," *IEEE Trans. Image Process.*, vol. 23, no. 7, pp. 3071–3084, Jul. 2014.

[29] L. Liu, S. Lao, P. W. Fieguth, Y. Guo, X. Wang, and M. Pietikäinen, "Median robust extended local binary pattern for texture classification," *IEEE Trans. Image Process.*, vol. 25, no. 3, pp. 1368–1381, Mar. 2016.

[30] Z. Pan, X. Wu, Z. Li, and Z. Zhou, "Local adaptive binary patterns using diamond sampling structure for texture classification," *IEEE Signal Process. Lett.*, vol. 24, no. 6, pp. 828–832, Jun. 2017.

[31] T. Ojala, T. Maenpaa, M. Pietikainen, J. Viertola, J. Kyllonen, and S. Huovinen, "Outex-new framework for empirical evaluation of texture analysis algorithms," in *Proc. 16th Int. Conf. Pattern Recognit.*, vol. 1, Aug. 2002, pp. 701–706.

[32] P. Brodatz, *Textures: A Photographic Album for Artists and Designers*. New York, NY, USA: Dover, 1966.

[33] K. J. Dana, B. van Ginneken, S. K. Nayar, and J. J. Koenderink, "Reflectance and texture of real-world surfaces," *ACM Trans. Graph.*, vol. 18, no. 1, pp. 1–34, Jan. 1999.

[34] S. Lazebnik, C. Schmid, and J. Ponce, "A sparse texture representation using local affine regions," *IEEE Trans. Pattern Anal. Mach. Intell.*, vol. 27, no. 8, pp. 1265–1278, Aug. 2005.

[35] E. Hayman, B. Caputo, M. Fritz, and J.-O. Eklundh, "On the significance of real-world conditions for material classification," in *Proc. Eur. Conf. Comput. Vis.*, 2004, pp. 253–266.

[36] A. Fathi and A. R. Naghsh-Nilchi, "Noise tolerant local binary pattern operator for efficient texture analysis," *Pattern Recognit. Lett.*, vol. 33, no. 9, pp. 1093–1100, Jul. 2012.

[37] Z. Guo, L. Zhang, and D. Zhang, "Rotation invariant texture classification using LBP variance (LBPV) with global matching," *Pattern Recognit.*, vol. 43, no. 3, pp. 706–719, 2010.

[38] S. Liao, M. W. K. Law, and A. C. S. Chung, "Dominant local binary patterns for texture classification," *IEEE Trans. Image Process.*, vol. 18, no. 5, pp. 1107–1118, May 2009.

[39] T. Ojala, M. Pietikäinen, and D. Harwood, "A comparative study of texture measures with classification based on featured distributions," *Pattern Recognit.*, vol. 29, no. 1, pp. 51–59, 1996.

[40] X. Tan and B. Triggs, "Enhanced local texture feature sets for face recognition under difficult lighting conditions," in *Proc. Int. Workshop Anal. Modeling Faces Gestures*, 2007, pp. 168–182.
[41] T. Song, H. Li, F. Meng, Q. Wu, and J. Cai, "LETRIST: Locally encoded transform feature histogram for rotation-invariant texture classification," *IEEE Trans. Circuits Syst. Video Technol.*, vol. 28, no. 7, pp. 1565–1579, Jul. 2018.
[42] M. Varma and A. Zisserman, "A statistical approach to texture classification from single images," *Int. J. Comput. Vis.*, vol. 62, nos. 1–2, pp. 61–81, 2005.
[43] M. Varma and A. Zisserman, "A statistical approach to material classification using image patch exemplars," *IEEE Trans. Pattern Anal. Mach. Intell.*, vol. 31, no. 11, pp. 2032–2047, Nov. 2009.
[44] K. Wang, C.-E. Bichot, C. Zhu, and B. Li, "Pixel to patch sampling structure and local neighboring intensity relationship patterns for texture classification," *IEEE Signal Process. Lett.*, vol. 20, no. 9, pp. 853–856, Sep. 2013.
[45] Z. Guo, Q. Li, J. You, D. Zhang, and W. Liu, "Local directional derivative pattern for rotation invariant texture classification," *Neural Comput. Appl.*, vol. 21, no. 8, pp. 1893–1904, 2012.
[46] R. Mehta and K. Egiazarian, "Dominant rotated local binary patterns (DRLBP) for texture classification," *Pattern Recognit. Lett.*, vol. 71, pp. 16–22, Feb. 2016.
[47] S. K. Roy, B. Chanda, B. B. Chaudhuri, D. K. Ghosh, and S. R. Dubey, "A complete dual-cross pattern for unconstrained texture classification," in *Proc. 4th IAPR Asian Conf. Pattern Recognit.*, Nanjing, China, Nov. 2017, pp. 741–746.
[48] S. K. Roy, B. Chanda, B. B. Chaudhuri, S. Banerjee, D. K. Ghosh, and S. R. Dubey, "Local directional ZigZag pattern: A rotation invariant descriptor for texture classification," *Pattern Recognit. Lett.*, vol. 108, pp. 23–30, Jun. 2018.
[49] S. K. Roy, S. R. Dubey, and B. B. Chaudhuri, "Local ZigZag max histograms of pooling pattern for texture classification," *Electron. Lett.*, vol. 55, no. 7, pp. 382–384, 2019.
[50] J. Ren, X. Jiang, and J. Yuan, "Noise-resistant local binary pattern with an embedded error-correction mechanism," *IEEE Trans. Image Process*, vol. 22, no. 10, pp. 4049–4060, Oct. 2013.
[51] L. Liu, P. Fieguth, Y. Guo, X. Wang, and M. Pietikäinen, "Local binary features for texture classification: Taxonomy and experimental study," *Pattern Recognit.*, vol. 62, pp. 135–160, Feb. 2017.
[52] Y. Zhao, D.-S. Huang, and W. Jia, "Completed local binary count for rotation invariant texture classification," *IEEE Trans. Image Process.*, vol. 21, no. 10, pp. 4492–4497, Oct. 2012.
[53] Z. Guo, X. Wang, J. Zhou, and J. You, "Robust texture image representation by scale selective local binary patterns," *IEEE Trans. Image Process.*, vol. 25, no. 2, pp. 687–699, Feb. 2015.
[54] T. Ahonen, J. Matas, C. He, and M. Pietikäinen, "Rotation invariant image description with local binary pattern histogram Fourier features," in *Image Analysis*. Berlin, Germany: Springer, 2009, pp. 61–70.
[55] R. Nosaka, Y. Ohkawa, and K. Fukui, "Feature extraction based on co-occurrence of adjacent local binary patterns," in *Proc. Pacific-Rim Symp. Image Video Technol.*, 2011, pp. 82–91.
[56] S. K. Roy, B. Chanda, B. B. Chaudhuri, D. K. Ghosh, and S. R. Dubey, "Local morphological pattern: A scale space shape descriptor for texture classification," *Digit. Signal Process.*, vol. 82, pp. 152–165, Nov. 2018.

FAWAD received the B.S. degree in telecommunication from the National University of Modern Languages, Pakistan, in 2011, and the M.S. degree from the Military College of Signals, National University of Science and Technology, Pakistan, in 2016, which was followed by his Graduate Assistant job with the Ghulam Ishaq Khan Institute of Engineering Sciences and Technology. He is currently pursuing the Ph.D. degree in telecommunication engineering with the University of Engineering and Technology Taxila, Pakistan. In 2012, he joined Zong China mobile company as a Transmission Engineer. His research interests include computer vision, pattern recognition, and image processing.

MUHAMMAD JAMIL KHAN received the B.Sc. degree in computer engineering, the M.Sc. degree in telecommunication engineering, and the Ph.D. degree in computer engineering from the University of Engineering and Technology Taxila, Pakistan, in 2005, 2009, and 2016, respectively, where he is currently an Assistant Professor and the Director of the Embedded Systems and Digital Signal Processing Laboratory. He is also the Founder of the Virtual Reality Simulation Laboratory, University of Engineering and Technology Taxila. He has authored or coauthored numerous technical articles in well-known international journals and conferences. His current research interests include multimedia content analysis, RF identification, and machine learning.

MUHAMMAD ALI RIAZ received the M.S. and B.S. degrees in electrical engineering from Iowa State University, USA, in 2010 and 2009, respectively. Afterward, he joined the Department of Electrical and Computer Engineering, Iowa State University, USA, as a Research Assistant. He is currently serving as an Assistant Professor with ACTSENA Research Group, University of Engineering and Technology Taxila. He is working towards the design and implementation of chipless RFID tags based on electromagnetic signature and their signal processing applications. He also serves as the Director of the Electronics and Measurements Laboratory, University of Engineering and Technology Taxila. His research work has been featured in a number of ISI-indexed journals.

HUMAYUN SHAHID received the B.S. degree in communication systems engineering from the Institute of Space Technology, Islamabad, in 2008, the M.S. degree in signal processing from Nanyang Technological University, Singapore, in 2011. He joined the Space and Upper Atmosphere Research Commission (SUPARCO), where he involved in radiation-hardened space grade components for telemetry subsystems. He joined the Department of Telecommunication Engineering, University of Engineering and Technology Taxila, where he is currently an Assistant Professor. He is with the ACTSENA Research Group working towards design and signal processing-related aspects of electromagnetic transduction-based sensor-incorporated chipless RFID tags. He is also the Director with the Departmental Antenna and RF Laboratory. His research work has been featured in a number of ISI-indexed journals and international conferences.

MANSOOR SHAUKAT KHAN received the B.Sc. degree from PU Lahore, Pakistan, in 1994, the M.Sc. degree in statistics from the University of ARID Agriculture Rawalpindi, Pakistan, in 2000, and the Ph.D. degree from the Beijing Institute of Technology (BIT), China, in 2016. He is currently an Assistant Professor with the Department of Mathematics, COMSATS University Islamabad, Pakistan. He has more than 10 research papers in reputed journals and proceedings of international conferences. His research interests include mathematical modeling and optimization, quality and reliability engineering, survival analysis, spatial data analysis, and data science. Most recently, he received the National Research Program for Universities Award from HEC Pakistan.

YASAR AMIN received the B.Sc. degree in electrical engineering with specialization in telecommunication and the M.B.A. degree in innovation and growth from the Turku School of Economics, University of Turku, Finland, and the M.Sc. degree in electrical engineering with specialization in system on chip design, and the Ph.D. degree in electronic and computer systems from the Royal Institute of Technology (KTH), Sweden, with the research focuses on printable green RFID antennas for embedded sensors. He is currently an Associate Professor and the Chairman of the Telecommunication Engineering Department, University of Engineering and Technology Taxila, Pakistan. He also serves as the Director of the Embedded Systems Research and Development Centre. He is the Founder of the Agile Creative Technologies for Smart Electromagnetic Novel Applications (ACTSENA) Research Group. He has authored or coauthored more than 100 international technical papers in conferences and journals. His research interests include the design and application of multiple antenna systems for next generation mobile communication systems, millimeter-wave and terahertz antenna array, implantable & wearable electronics, and inkjet printing technology in microwave applications. He is a member of more than 12 international professional societies and the fellow of PAE.

JONATHAN LOO received the M.Sc. degree in electronics and the Ph.D. degree in electronics and communications from the University of Hertfordshire, U.K., in 1998 and 2003, respectively. He leads a research team of 8 Ph.D. students in the area of communication and networking. He is currently a Professor and the Chair in computing and communication engineering with the School of Computing and Engineering, University of West London, U.K. His research interests include network architecture, communication protocols, network security, embedded systems, video coding and transmission, wireless communications, digital signal processing, and optical networks. He has successfully graduated 13 Ph.D. students as a Principle Supervisor and contributed over 175 publications in the aforementioned specialist areas.

HANNU TENHUNEN is currently a Chair Professor of electronic systems with the Royal Institute of Technology (KTH), Stockholm, Sweden. He has been a Full Professor, an Invited Professor, or Visiting Honorary Professor with TUT and UTU, Finland, KTH, Sweden, Cornel U, USA, INPG, France, Fudan and Beijing Jiaotong Universities, China, and Chinese University of Hong Kong, Hong Kong, and has an Honorary Doctorate from Tallinn Technical University. He has been the Director of multiple national large-scale research programs or being an initiator and director of national or European Graduate Schools. He has actively contributed to VLSI and SoC design in Finland and Sweden via creating new educational programs and research directions, most lately at European level as being the EU-level Education Director of the new European flagship initiative European Institute of Technology and Innovations (EIT), and its Knowledge and Innovation Community EIT ICT Labs. He is the founding editorial board member of three scientific journals and a guest editor for multiple special issues of scientific journals and books. He has authored or coauthored more than 900 international technical papers in conferences and journals. He has been granted nine foreign patents. He is a member of the Academy of Engineering Science of Finland.